

RADIO – OPTICAL CORRELATIONS IN HIGH-Z RADIO GALAXIES AND QUASARS

Chris J. Willott¹

Abstract

The narrow emission line luminosities of radio-loud AGN are well-correlated with their low-frequency radio luminosities. This correlation is linear and extends over at least four orders of magnitude. The correlation is discussed in terms of a linear relationship between the power in the radio-emitting jets and the photoionizing (i.e. accretion) luminosity. Support for this theory comes from a direct correlation between the optical continuum and radio luminosities of steep-spectrum quasars. We discuss the dependence of the observed luminosities of AGN on their black hole masses and how close to the Eddington limit they are accreting.

1 Introduction

Despite all the observational effort which has gone into researching extragalactic radio sources, there are still major uncertainties regarding their fueling, radiation emission mechanisms and the relationship between the active nuclei, host galaxies and larger-scale environments. Since resolving the various central emission components in most wavebands is still difficult, much progress has been made by looking for correlations between observables. The multi-waveband spectra of AGN give considerable scope for such studies. In this paper I consider correlations between the low-frequency (i.e. lobe-dominated) radio emission and optical quantities such as the optical continuum and emission lines. These are particularly revealing since, unlike many observables which are correlated due to reprocessing of radiation from one form to another, the emission regions and mechanisms are physically distinct and therefore telling us something more fundamental about the way that active galaxies are powered.

¹ Astrophysics, Department of Physics, Keble Road, Oxford, OX1 3RH, U.K.

Radio sources can be crudely split into two groups with different radio structures and luminosities: the low luminosity (monochromatic 151 MHz luminosity $L_{151} \lesssim 10^{25} \text{ WHz}^{-1}\text{sr}^{-1}$), edge-darkened FRIs and the high luminosity, edge-brightened FRIIs (also known as ‘classical doubles’). In this paper I will concentrate on the FRII class of which much larger and more complete samples exist. Unified schemes have been extremely successful in describing the different properties of powerful FRII radio galaxies and quasars as due to a difference in the angle between the line-of-sight and the jet axis (see Antonucci 1993 for a review of this subject). Both the extended radio emission and (at least the majority of) the narrow line emission of both quasars and radio galaxies are expected to be emitted isotropically in such models. The cosmology assumed (except where stated otherwise) is that $H_0 = 50 \text{ km s}^{-1}\text{Mpc}^{-1}$, $\Omega_M = 1$, and there is zero cosmological constant.

2 Optical continuum and radio emission in steep-spectrum quasars

There have been varied results over the past 20 years with respect to the existence of a correlation between the optical and radio luminosities of radio-loud quasars due to:

- Inhomogeneous samples with unknown selection effects
- Small complete samples with small range in radio luminosity
- Flat-spectrum quasars may have a correlation due to beaming of optical and radio flux

One must also be able to differentiate between luminosity dependence and evolution. In any single flux-limited sample, the steepness of the luminosity function ensures a tight luminosity-redshift correlation so that the most luminous sources in the sample will generally be those at the highest redshifts. Breaking this degeneracy requires combining several samples selected in a similar manner with different flux limits.

Browne & Murphy (1987) found a correlation between the optical and radio luminosities in a large, but inhomogeneous sample. Baker (1997) showed that the optical continua of quasars with stronger radio cores are brighter than those with weak cores and that emission line equivalent widths anti-correlate with R (the ratio of core to extended flux). These observations can be explained as a combination of optical beaming and anisotropic optical continuum - e.g. a disk or reddening.

To understand the situation properly requires samples of quasars selected in an orientation-independent manner. Serjeant et al. (1998) used low-frequency selected complete samples (178 & 408 MHz) to show that there is a correlation between the radio luminosity at low-frequency and the optical continuum luminosity (Fig. 1). The Serjeant et al. best-fit relation gives $L_{\text{opt}} \propto L_{\text{rad}}^{0.6 \pm 0.1}$ with dispersion of 1.6 mag.

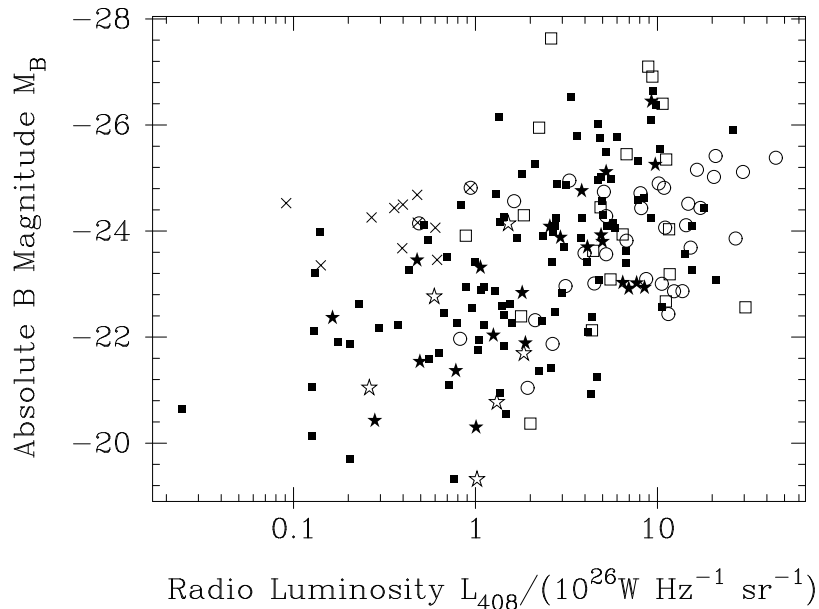


Fig. 1. Radio luminosity against absolute magnitude for steep-spectrum quasars (SSQs) from the MAQS (squares), the MQS (stars) (which both have flux-limits of $S_{408} = 0.95$ Jy) and 3CRR (circles). This plot is reproduced from Serjeant et al. (1998) and assumes $H_0 = 100 \text{ km s}^{-1} \text{ Mpc}^{-1}$.

This correlation is also seen in a combination of 3CRR (178 MHz – Laing, Riley & Longair 1983) and 7CRS (151 MHz) complete (no optical magnitude limit) SSQ samples (Willott et al. 1998). In the redshift range $1 < z < 2$, where there is the largest overlap between quasars in the two samples, it is clear that the 3CRR sources (with radio luminosities ~ 25 times higher than 7CRS sources) are more luminous in the optical (Fig. 2). The mean M_B for 3CRR SSQs is -25.9 ± 0.2 mag, compared to -24.6 ± 0.3 for the 7CRS SSQs. This shows a direct link between the optical continuum and extended radio emission mechanisms for quasars.

A consequence is that radio fainter samples will contain optically-fainter quasars. Therefore, despite the fact that all 3CRR quasars are identified on the POSS-I plates ($R \lesssim 20$), this should not be assumed for fainter radio samples (e.g. only 60% of quasars in the 7CRS are detected on the POSS-I plates).

3 Narrow-line emission in radio-loud AGN

The narrow-line region (NLR) in radio sources is extended over several kpc, beyond the proposed dusty torus which obscures the central continuum source and

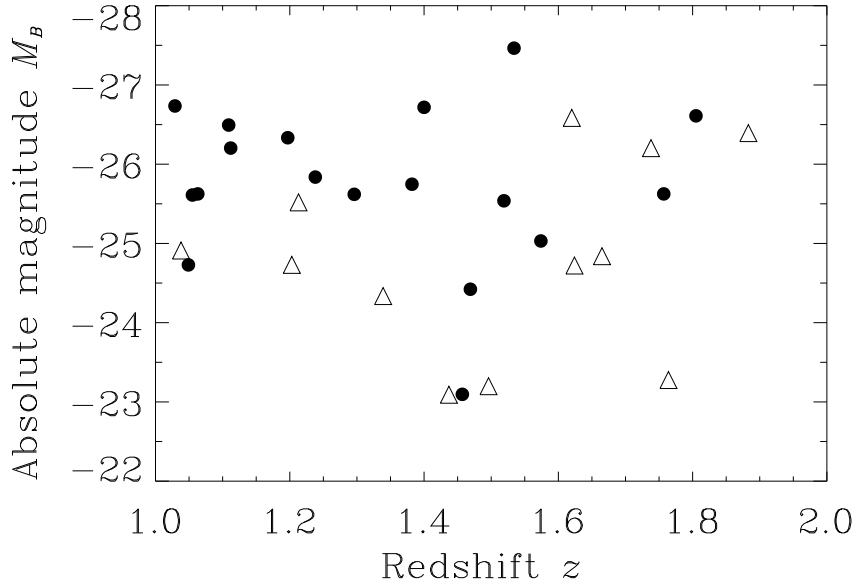


Fig. 2. Absolute magnitude against redshift for quasars in the 3CRR (circles) and 7CRS (triangles) complete samples with $1 < z < 2$. Note the vertical separation of the absolute magnitudes for the two samples.

broad-line region along certain lines-of-sight. Therefore the narrow-line emission is believed to be independent of the jet axis orientation. Similar distributions of narrow-line luminosities in samples of radio galaxies and quasars, matched in extended radio luminosity, have been suggested as a fundamental test of the unified schemes (e.g. Barthel 1989). In general the emission line luminosities of well-matched samples of radio galaxies and quasars are similar, in agreement with unified schemes. There is some evidence for higher [OIII] $\lambda 5007$ luminosities in quasars than radio galaxies, but see Simpson (1998) for a discussion of this and a possible resolution within the framework of unified schemes.

There is a strong positive correlation between the extended radio luminosities and narrow emission line luminosities of 3C radio sources (Baum & Heckman 1989; Rawlings et al. 1989). However, due to the correlation between radio luminosity and redshift in any single flux-limited sample, this could equally be interpreted as a correlation between redshift and emission line luminosity. Using the low-frequency selected 7CRS in combination with the 3CRR sample, Willott et al. (1999) confirmed that the correlation is predominantly with radio luminosity (although a weak residual correlation with redshift remains). Fig. 3 plots the [OII] $\lambda 3727$ line luminosity against low-frequency radio luminosity for these samples (also included is the 6CE complete sample which has flux-limits in between the 3CRR and 7CRS

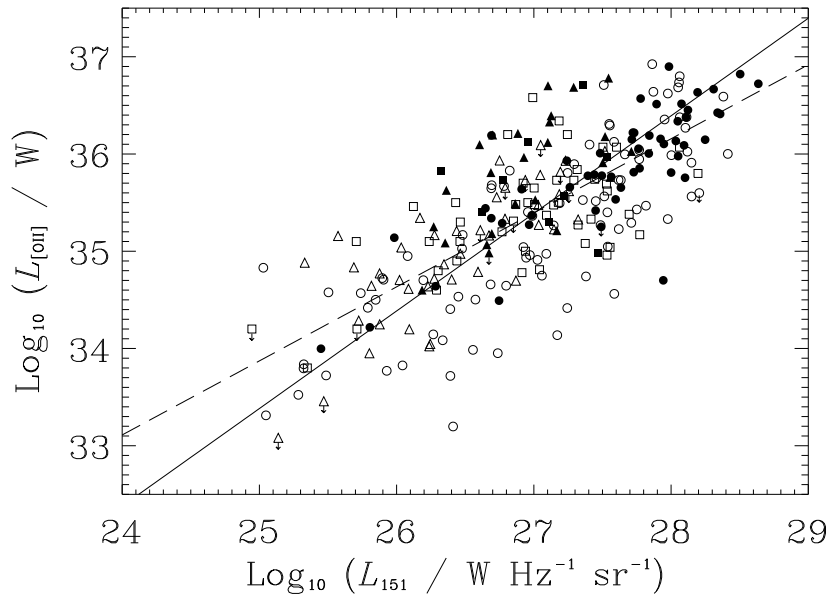


Fig. 3. The correlation between narrow [OII] emission line luminosity and low-frequency radio luminosity for FR II radio sources in the 3CRR (circles), 6CE (squares) and 7CRS (triangles) complete samples. Quasars (and broad-lined radio galaxies) are shown as open symbols and radio galaxies as filled symbols. Note that the [OII] flux was not available for every object, so for about a third of these objects another line was measured and the [OII] flux inferred using the line ratios in McCarthy (1993). The dashed line is a standard least-squares linear fit to the data and the solid line a fit minimizing the deviations along both axes.

samples - see Rawlings, Eales & Lacy 2000). As expected, the 6CE sources follow the same correlation as the 3CRR and 7C sources.

3.1 Slope

Modeling the interpretation of this correlation requires the relationship between the two variables to be quantified. There is no apparent change in the slope of the correlation over the four orders of magnitude shown in Fig. 3. To determine the slope a linear least-squares fit is carried out in logarithm space. The best-fit slope is 0.76 ± 0.04 (dashed line) – not very different from that of 0.79 ± 0.04 determined in Willott et al. (1999) without the 6CE sample. The standard least-squares fit only minimizes the sum of the square of the deviations of the model from the data along one axis – in this case $\log_{10} L_{[\text{OII}]}$. However, when one is dealing with correlations between quantities such as two fluxes or two luminosities which

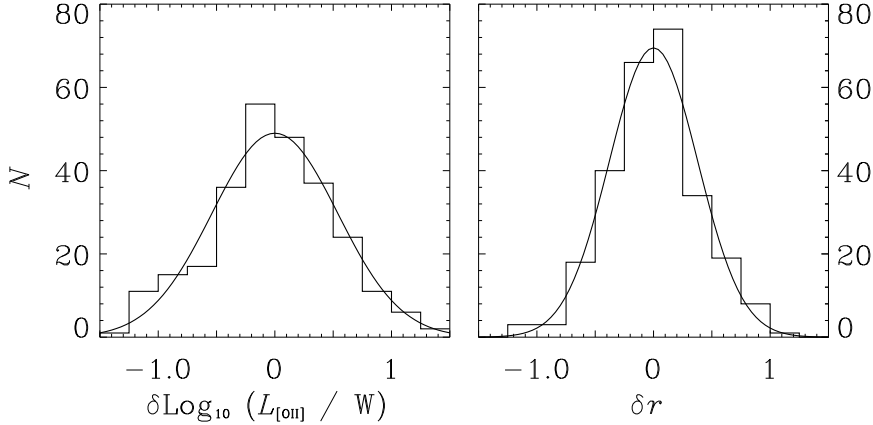


Fig. 4. Histograms of the scatter about the best-fit power-law relationship between $L_{[\text{OII}]}$ and L_{151} (solid line in Fig. 3). The left-hand side plots the scatter in $\log_{10} L_{[\text{OII}]}$ and the right-hand side shows the scatter in a direction perpendicular to the best-fit line. Both distributions are close approximations to gaussians.

show scatter, the true relationship between the quantities can only be obtained by minimizing the deviations along both axes simultaneously. As an example we find that by performing a least-squares fit minimizing the square of the deviations along the other axis (i.e. $\log_{10} L_{151}$), the slope of the correlation is now 1.33 ± 0.07 . The large difference between these two values of the slope shows just how important this effect is in this type of situation. A fit simultaneously minimizing the sum of the squares of the deviations along both axes gives a slope of 1.00 ± 0.04 and is also shown on Fig. 3 (solid line). Thus we find a direct proportionality between the narrow-line luminosity and radio luminosity.

3.2 Scatter

This linear relationship between narrow line luminosity and radio luminosity is intriguing, but we should never lose sight of the fact that, as Fig. 3 shows, there is considerable scatter about this relationship. Fig. 4 shows a histogram of the residuals between the data and the best-fit slope of 1.00. On the left-hand side are the residuals in $\log_{10} L_{[\text{OII}]}$. This is the scatter in the values of $\log_{10} L_{[\text{OII}]}$ for a given radio luminosity. The distribution of residuals is close to gaussian (in log space) with $\sigma = 0.54$, i.e. $\pm 1\sigma$ is one order of magnitude in $L_{[\text{OII}]}$. However, the true scatter about the best-fit relationship is better defined in terms of the smallest deviation of the data from the best-fit line (which we call δr). The values of δr are lower than the values of $\delta \log_{10} L_{[\text{OII}]}$ by a factor $\sin(\tan^{-1}(1.0/\text{slope}))$. For the slope of 1.00 we find the residuals δr are lower by a factor of 0.7 leading to a gaussian distribution with $\sigma = 0.38$ (right-hand side of Fig. 4). There are

various factors which can account for the scatter in this correlation such as ranges in radio source environments, NLR ionization states and NLR covering factors (see Willott et al. 1999 for a more detailed discussion).

4 Interpretation of radio – optical correlations

In the previous section we found that the correlation between narrow emission line and radio luminosity extends over four orders of magnitude with a linear slope. Interpretation of this correlation requires 3 questions to be answered.

4.1 What determines low-frequency radio luminosity?

The radio luminosity of FRII radio sources at low-frequencies (< 1 GHz) is dominated by the extended lobes. These lobes are fed by relativistic particles accelerated in the hotspots which cool via synchrotron radiation. However, the radio luminosity emitted is only a small fraction of the total kinetic power of the jets, Q_{jets} . A much greater fraction is stored in the lobes and/or lost to the environment via work done by the expanding radio source (Scheuer 1974). Models of the evolution of FRII sources lead to a nearly linear relationship between Q_{jets} and L_{151} (e.g. $Q_{\text{jets}} \propto L_{151}^{6/7}$ in the models of Rawlings & Saunders 1991 and Kaiser & Alexander 1997). These models also show that there is only a weak negative dependence of the radio luminosity upon source size (however, at large sizes the luminosity may undergo a rapid decrease due to increased adiabatic and synchrotron losses – Kaiser, Dennett-Thorpe & Alexander 1997; Blundell, Rawlings & Willott 1999).

4.2 What is the NLR ionization mechanism?

The presence of high-excitation lines in radio galaxy and quasar narrow-line spectra indicates that the active nucleus is the major source of ionization in these objects. There are several possible ionization mechanisms: photoionization, jet-cloud collisions and shock-excitation. Photoionization by the central source is believed to be the primary ionization mechanism for the majority of objects. Studies of line ratios show shock-excitation is important for some sources (Clark et al. 1997; Villar-Martin et al. 1999). However, shocks have more effect on the morphology, kinematics and ionization state than on the overall line luminosity. Interestingly, Best, Röttgering & Longair (2000) have found that the $z \sim 1$ 3CRR radio galaxies with line emission matching the shock models also tend to have the smallest radio sources. This implies that for some small radio sources the passage of the jet through the narrow line region can cause excess emission with a low-ionization state. Willott et al. (1999) found a weak residual anti-correlation between emission line luminosity and radio source linear size. This showed up as a lack of sources with weak lines and small sizes, consistent with the results of Best et al. However, in general photoionization is the most likely mechanism for exciting the lines

in most radio sources (see discussion in Willott et al. 1999). In the ionization-bounded case, where individual optically-thick clouds absorb and re-radiate all the incident flux, the narrow-line luminosity is proportional to the photoionizing quasar luminosity Q_{phot} .

4.3 What drives the luminosities?

The low-frequency radio luminosity has a nearly linear relationship with the bulk kinetic power in the jets Q_{jets} . The narrow emission line luminosity is proportional to the photoionizing quasar luminosity Q_{phot} . This allows us to interpret the observed linear correlation between narrow line and radio luminosity as a linear correlation between Q_{jets} and Q_{phot} . Note that the correlation between the optical and radio luminosities of steep-spectrum quasars in Section 2 strongly supports this interpretation. This rules out effects such as the environment controlling both the radio and narrow-line luminosities. Although there are large uncertainties in the absolute normalization between radio luminosity and Q_{jets} , Willott et al. (1999) found that $0.05 \lesssim Q_{\text{jets}}/Q_{\text{phot}} \lesssim 1$, so that the jet power is within about an order of magnitude of the UV luminosity. Celotti et al. (1997) found a relationship between the kinetic energy in parsec-scale jets and the broad emission line luminosities of quasars. This study also showed that the ionizing luminosity is of the same order of magnitude as the jet power.

What are the properties of the AGN that determine Q_{phot} and Q_{jets} ? Although there is still debate about the exact UV emission process in AGN – accretion disk or free-free emission (e.g. Siemiginowska et al. 1995), the energy source is the release of energy as material falls into the deep potential well close to a supermassive black hole. Using the fact that there is an upper limit to the ionizing luminosity which can be emitted by a black hole of a certain mass – the Eddington limit L_{Edd} – the luminosity can be related to the black hole mass M_{BH} via $Q_{\text{phot}} \propto f_{\text{Edd}} M_{\text{BH}}$ where f_{Edd} is the fraction of the Eddington luminosity being emitted, i.e. $Q_{\text{phot}}/L_{\text{Edd}}$ (we are neglecting here the infrared contribution to the bolometric luminosity, which is of the same order as Q_{phot}). What determines the range of four orders of magnitude in Q_{phot} in Fig. 3? Is it a similar size range in M_{BH} or f_{Edd} . The answer is that both play significant and probably equal parts in determining the range of observed luminosities. The objects with the highest values of Q_{phot} in Fig. 3 have similar luminosities to the most luminous radio-quiet (optically-selected) quasars. It seems likely that these objects are emitting at approximately the Eddington limit ($f_{\text{Edd}} \sim 1$) leading to black hole masses $\sim 10^9 - 10^{10} M_{\odot}$.

Reverberation studies of low-redshift low-luminosity quasars give the best estimates currently available of the range of black hole masses in these objects. Kaspi et al. (2000) present data on the largest sample of objects to date – the results of which are shown in Fig. 5. These objects (Seyfert 1s and quasars) have black hole masses in the range $10^6 - 10^9 M_{\odot}$ and $f_{\text{Edd}} \sim 0.01 - 1$. There is evidence for a correlation between Q_{phot} and f_{Edd} , but no correlation between M_{BH} and f_{Edd} . Thus the range in AGN luminosity is due to similar size ranges in both M_{BH} and f_{Edd} . Note that the most luminous sources in Fig. 3 are an order of magnitude

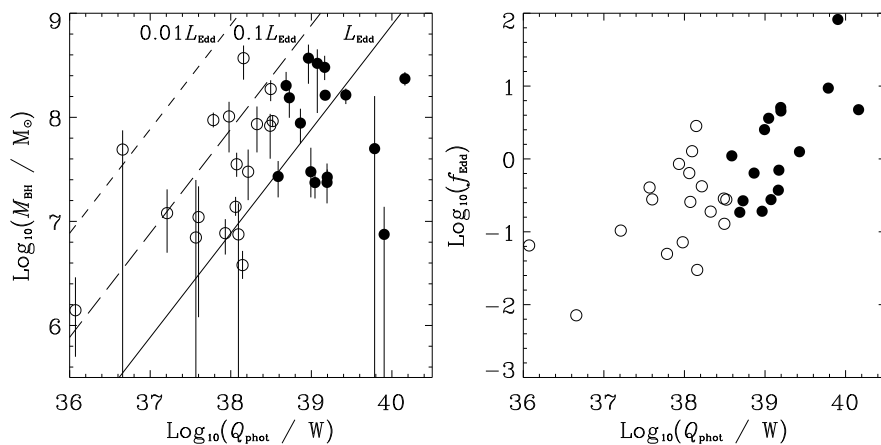


Fig. 5. Reverberation data of low-redshift, low-luminosity quasars ($M_B < -23$ – filled symbols) and Seyfert 1 galaxies (open symbols) from Kaspi et al. (2000) converted to our assumed value of the Hubble constant $H_0 = 50 \text{ km s}^{-1} \text{ Mpc}^{-1}$. The left-hand plot shows black hole mass M_{BH} against Q_{phot} [calculated assuming a bolometric correction of $Q_{\text{phot}} = 10\lambda L_{\lambda}(5100 \text{ \AA})$ as in Wandel, Peterson & Malkan 1999]. The right-hand plot shows f_{Edd} against Q_{phot} for the same data (error bars omitted for clarity). Note the positive correlation in this data.

more luminous than that yet sampled by reverberation data and long-term ($\gtrsim 10$ yr) monitoring of high-luminosity quasars is needed to measure their broad-line region sizes and black hole masses.

It is now well-established that many nearby galaxies (including our own) contain large central mass concentrations, most probably in the form of supermassive black holes (e.g. Richstone et al. 1998) and that the masses of these black holes are linearly correlated with the galaxy bulge masses (Magorrian et al. 1998). A similar correlation is also seen for AGN with reverberation black hole masses (Wandel 1999). Roche, Eales & Rawlings (1998) find that 6C radio galaxies at $z \sim 1$ are smaller and fainter than 3CR galaxies (Best, Longair & Röttgering 1998) at the same redshift (which are a factor of about 6 times greater in radio luminosity). They conclude that there is indeed a positive correlation between the radio luminosity and host galaxy luminosity, which would seem to be caused by both quantities correlating with black hole mass. The lack of such correlations at low redshift (e.g. Eales et al. 1997) can be explained because the fuel supply is more limited due to the virialization of galaxies and clusters (e.g. Rees 1990) and the decrease in the galaxy merger rate (Le Fèvre et al. 2000).

Acknowledgements

Thanks to my collaborators Steve Rawlings, Katherine Blundell and Mark Lacy for their work on the 7C Redshift Survey. Extra thanks to Steve Rawlings for a critical reading of this manuscript.

References

- Baker J.C., 1997, MNRAS, 286, 23
Barthel P.D., 1989, ApJ, 336, 606
Baum S.A., Heckman T.M., 1989, ApJ, 336, 702
Best P.N., Longair M.S., Röttgering H.J.A., 1998, MNRAS, 295, 549
Best P.N., Röttgering H.J.A., Longair M.S., 2000, MNRAS, 311, 23
Blundell K.M., Rawlings S., Willott C.J., 1999, AJ, 117, 677
Browne I.W.A., Murphy D., 1987, MNRAS, 226, 601
Celotti A., Padovani P., Ghisellini G., 1997, MNRAS, 286, 415
Clark N.E. *et al.* 1997, MNRAS, 286, 558
Eales S.A. *et al.* 1997, MNRAS, 291, 593
Kaiser C.R., Alexander P., 1997, MNRAS, 286, 215
Kaiser C.R., Dennett-Thorpe J., Alexander P., 1997, MNRAS, 292, 723
Kaspi S. *et al.* 2000, ApJ, 533, 631
Laing R.A., Riley J.M., Longair M.S., 1983, MNRAS, 204, 151
Le Fèvre O. *et al.* 2000, MNRAS, 311, 565
Magorrian J. *et al.* 1998, AJ, 115, 2285
McCarthy P.J., 1993, ARAA, 31, 639
Rawlings S., Saunders R., 1991, Nature, 349, 138
Rawlings S., Saunders R., Eales S.A., Mackay C.D., 1989, MNRAS, 240, 701
Rawlings S., Eales S.A., Lacy M., 2000, MNRAS, submitted
Rees M.J., 1990, Science, 247, 817
Richstone D., *et al.* 1998, Nature, 395, A14
Roche N., Eales S.A., Rawlings S., 1998, MNRAS, 297, 405
Scheuer P.A.G., 1974, MNRAS, 166, 513
Serjeant S. *et al.* 1998, MNRAS, 294, 494
Siemiginowska A. *et al.* 1995, ApJ, 454, 77
Simpson C., 1998, MNRAS, 297L, 39
Villar-Martin M., Tadhunter C.N., Clark N. E., 1997, A&A, 323, 21
Wandel A., 1999, ApJ, 519, L39
Wandel A., Peterson B.M., Malkan M.A., 1999, ApJ, 526, 579
Willott C.J., Rawlings S., Blundell K.M., Lacy M., 1998, MNRAS, 300, 625
Willott C.J., Rawlings S., Blundell K.M., Lacy M., 1999, MNRAS, 309, 1017